Journal of Cellular Biochemistry 101:1046–1061 (2007)

Evidence for the Existence of Satellite DNA-Containing Connection Between Metaphase Chromosomes

I.S. Kuznetsova,[1] N.I. Enukashvily,[1] E.M. Noniashvili,[2] A.N. Shatrova,[1] N.D. Aksenov,[1] V.V. Zenin,[1] A.P. Dyban,[2] and O.I. Podgornaya[1]*

[1]Institute of Cytology RAS, Tikhoretsky Avenue 4, St. Petersburg 194064, Russia
[2]Research Institute for Experimental Medicine RAMS, Akademika Pavlova Street 12, St. Petersburg 197376, Russia

Abstract Physical connections between mitotic chromosomes have been reported previously. It was assumed that the interchromosome connection was based on the DNA-protein thread. However, the data about DNA sequences and protein component in the thread is fragmentary. We demonstrated on the mouse cultured cell line and prematurely condensed chromosomes that: (a) all four mouse satellite DNA fragments (major and minor satellite, mouse satellite 3 (MS3) and mouse satellite 4 (MS4)) were involved in the thread formation; (b) MS4 was involved in the thread to the least extent among all the other fragments; (c) telomere was never a member of the thread; (d) the thread was synthesized at a late G_2 phase; (e) RNA helicase p68 and CENP-B were among the protein components of the interchromosome connection. It was shown by FACS analysis that in mouse and human cell lines: (1) the flow karyotype spectrums were never free from chromosome aggregates; (2) chromosome association did not depend on the chromosome length and each chromosome was free to associate with the other. J. Cell. Biochem. 101: 1046–1061, 2007. © 2007 Wiley-Liss, Inc.

Key words: interchromosome connection; satellite DNA; RNA helicase p68; FACS

Physical connections between chromosomes have previously been reported [Maniotis et al., 1997a], and shown to be neither artifact of colchicine nor of hypotonic treatment [Takayama, 1975; Chiarelli et al., 1977]. It has been demonstrated that the interchromosome connection in mammalian cells can be completely destroyed with DNAse [Maniotis et al., 1997a] but when treated with RNAse or pepsin it becomes more rigid [Hoskins, 1968]. Electron micrograph studies have shown four groups of fibers attached to the centromere (CEN) in both mouse and human chromosomes. Each of these threads is composed of DNA fibers of 100 Å wound around a proteinaceous thread of 600 Å [Hoskins, 1968].

Micromechanical studies of mitotic chromosomes with DNA-cutting enzymes reveal that the element, which gives mitotic chromosomes their mechanical integrity, is DNA itself. These experiments indicate that chromatin-condensing proteins are not organized into a mechanically contiguous "scaffold," but instead that the mitotic chromosomes are best thought of as a cross-linked network of chromatin [Poirier and Marko, 2002]. Interchromosome fibers between mitotic chromosomes have repeatedly been observed in this work.

The data about RNA or DNA sequences in the thread is fragmentary, not to mention the protein component. The most probable DNA in the thread is satellite DNA (satDNA). The well-characterized CEN satDNA fragment FCP in the chaffinch (*Fringilla coelebs PstI*) has been shown to be a constituent of the thread connecting chromosomes by primed in situ hybridization (PRINS) and fluorescent *in situ* hybridization (FISH) [Saifitdinova et al., 2001].

Grant sponsor: HUGO DOE, USA (to O.I.P.); Grant number: OR00033-93CIS008; Grant sponsor: INTAS; Grant number: 94-22882; Grant sponsor: Russian Foundation for Basic Research; Grant numbers: 04-04-48993-a, 05-04-49156-a, 04-04-48734-a; Grant sponsor: The RF President Council; Grant numbers: MK-2497.2005, MK-1187.2006.4; Grant sponsor: The program grant of RAS "Molecular and Cell Biology."

*Correspondence to: O.I. Podgornaya, Institute of Cytology RAS, Tikhoretsky Avenue 4, St. Petersburg 194064, Russia. E-mail: podg@IM1632.spb.edu

Received 1 June 2006; Accepted 16 November 2006

DOI 10.1002/jcb.21237

On the basis of their experimental findings, the authors suggest a role for DNA–protein interaction in the thread formation.

Four satDNA fragments were used in the current work: AT-rich major (MaSat) and minor (MiSat) satellites, and CG-rich—Mouse Satellite 3 (MS3) and Mouse Satellite 4 (MS4). Two classes of satDNA termed MaSat and MiSat were found in the pericentromeric (periCEN) and CEN regions, respectively, in *Mus musculus*. MiSat is separated from the euchromatin of the long arm by a large domain consisting of the MaSat array in the amount 10–20 times higher than MiSat [Mitchell et al., 1996]. MiSat possesses the binding site for CENP-B—CENP-B-box [Kipling et al., 1995]. MS3 and MS4 fragments have recently been isolated and characterized [Kuznetsova et al., 2005]. Of the total DNA, 2.2% consists of MS3 while MS4 accounts for 1.6% of the total DNA. On metaphase chromosomes, MS3 and MS4 are located in the CEN and periCEN regions, respectively [Kuznetsova et al., 2005].

In the present study, we checked the satDNA-binding protein such as CENP-B and RNA helicase p68. CENP-B is one of the most well characterized satDNA binding proteins [Earnshaw et al., 1989; Sugimoto et al., 1998]. RNA helicase p68 is a protein binding three different satDNA probes in vitro: human satellite 3 [HS3; Podgornaya et al., 2000], alphoid fragment [Enukashvily et al., 2000], and mouse MiSat [Enukashvily et al., 2005].

It is hypothesized that fibers between chromosomes are telomeric (Tel) structures because the interchromosome fibers at metaphase almost always come from chromosome ends [Poirier and Marko, 2002], and therefore probes for Tel DNA need to be tested. Most of the work cited is done on tumor cell lines, so the authors pose the question as to whether these fibers are intrinsic to transformed cells and suggest parallel studies in primary cell cultures [Poirier and Marko, 2002]. Following these suggestions we used a Tel fragment as a probe in the current work.

The aim of our work was to trace the thread in vivo and in vitro and to find out what satDNA and satDNA-binding proteins were involved in the thread structure. We found that the thread between chromosomes exists in each mitotic ring *in vitro* in all the cultured cells tested, whether malignant or normal. Also, chromosome association does not depend on the chromosome length and is random for each chromosome. The thread composition of satDNA and CENP-B and RNA helicase p68 has been confirmed, though the Tel fragment was never involved in the thread formation.

MATERIALS AND METHODS

Plasmids and Probes

The following DNA fragments were used: a fragment (471 bp) of MaSat [Radic et al., 1987] cloned into pBluescriptIIKS$^+$, a MiSat fragment (362 bp) inserted in pGEM7 vector [Kipling et al., 1995], fragments MS3 (300 bp) and MS4 (600 bp) cloned into pUC19 vector [Kuznetsova et al., 2005]. The $(TTAGGG)_3$ oligonucleotide 5′ fluorescent-labeled telomere probe was also used.

Fragments of MaSat, MiSat, MS3, and MS4 were labeled with digoxigenin-11-dUTP (DIG), biotin16-dUTP, Cy3-dUTP, and Cy5-dUTP (Roche), for FISH. The labeled nucleotides were incorporated into fragments by PCR, using M13 forward and reverse primers.

Cell Cultures and Slide Preparation

The human spontaneously transformed lymphoblastoid cell line (GM-130) was provided by Los Alamos National Laboratory, human primary lung fibroblasts (FLECH) were provided by Influenza Institute RAMN (St. Petersburg, Russia), human epidermoid carcinoma of larynx (Hep-2), mouse fibroblast-like cells of line NCTC clone 929 clone L (L929) were provided by the Institute of Cytology RAS (St. Petersburg, Russia). The cells were cultured under standard conditions in DMEM medium supplemented with 10% fetal calf serum. Preparations were fixed in methanol:acetic acid (3:1), for FISH or in 3% formaldehyde in KCM buffer (135 mM KCl, 20 mM NaCl, 0.5 mM EDTA, 0.1% Triton X-100, 10 mM Tris-HCl, pH 8.0; Gooderham and Jeppesen, 1983) for 10 min, for immunostaining.

Cell Synchronization

L929 cells were synchronized in G_0/G_1, S, and G_2 as described [Dolnik et al., 2003; Enukashvily et al., 2005]. Cells in G_0/G_1, S, and G_2/M phases were determined by fluorescence-activated cell sorting (FACS) analysis of parallel treated samples according to the standard protocol at ATC-3000 device (Odam-Bruker, France).

Prematurely Condensation of Chromosomes (PCC)

Female mice (10–12-weeks-old) F1(C57BL/CBA)BL were used. The pronuclei of one-cell stage embryos (first mitotic division, 26 h after the administration of human chorionic gonadotropin) were treated with ocadaic acid (final concentration 5 μM) to obtain prematurely condensed chromosome (PCC) preparations [Cohen et al., 1990; Dyban et al., 1993]. Subsequent treatment with series of fixatives containing methanol and acetic acid enables PCC preparations that are free of cytoplasmic contaminations, nuclear envelope, or nucleoplasmic contaminations to be obtained. On the slides used in the present work, the PCC were classified as G_2-chromosomes according to morphological criteria [Dyban et al., 1993].

Replication Sites Labeling With BrdU

Synchronized cells were cultured in the presence of 100 μM BrdU at 37°C for 15 min [O'Keefe et al., 1992] in certain intervals after the block release (16, 20, 24 h) and allowed to proceed up to metaphase plate formation. Metaphase chromosomes were isolated from cells blocked in mitosis by 0.5 mg/ml colcemid (Gibco). For the detection of labeled replication sites the plates were incubated with antibody (AB) to BrdU raised in mouse (1:200; Roche). Alexa Fluor™ 584 goat-anti-mouse IgG was used as a secondary AB (Molecular Probes).

Immunostaining

Slides were incubated with AB against CENP-B and RNA helicase p68. The AB against CENP-B raised in a rabbit was kindly provided by Dr. W. Earnshaw (Edinburgh University, Scotland) [Earnshaw et al., 1989]. The AB against RNA helicase p68 raised in guinea pig has been described [Enukashvily et al., 2000]. Alexa Fluor® 488 chicken anti-rabbit IgG and Alexa Fluor™ 584 goat-anti- guinea pig IgG (Molecular Probes) at 1:500 were used for the detection. Slides were counterstained in DAPI (0.5 μg/ml) and mounted in VectaShield (VectorLab).

Primed In Situ Labeling (PRINS)

The PRINS technique was used as described [Kuznetsova et al., 2005]. In the first cycle of two-color PRINS was carried out with an oligonucleotide corresponding to the MiSat sequence (5′-AAATCCCGTTTCCAACGAAT-3′) and (5′-TGGAAAATGATGAAAACCACA-3′); in this case the labeled nucleotide was biotin-16-dUTP (Roche). The second PRINS cycle was carried out with an oligonucleotide corresponding to MS3 (5′-TACGACTGGTGCG-TGGACA-3′) and (5′-GTAACCAGCGCCAT-CAGCTT-3′) and DIG-11-dUTP (Roche). Annealing and extension were carried out, respectively, at 53°C for 10 min, and 62°C for 40 min.

Fluorescent In Situ Hybridization (FISH)

The slides were denatured by pre-heating at 80°C for 5 min. The hybridization was performed with 70% formamide, 1 × Denhardt, 20 ng of each probe, 2 × SSC at 37°C overnight. After post-hybridization washes, the probes were detected with anti-digoxigenin-FITC for digoxigenin-labeled probes and with anti-avidin-Cy3.5 for biotin-labeled ones (Roche). Finally, the slides were counterstained in DAPI (0.5 μg/ml) and mounted in VectaShield (VectorLab).

The slides were examined using a DMRXA fluorescent microscope (Leica Wetzlar GmbH, Germany) equipped with a FLUOTAR ×100/1.30 objective, a 1.6× tube lens, a black-white CCD camera and the appropriate filter cubes. QFISH software (Leica Cambridge Ltd.) was used to acquire and process microscope images. The images were pseudocolored and prepared for publication using Adobe Photoshop software.

FLUORESCENCE-ACTIVATED CELL SORTING (FASC) BASED METHODS

Chromosome Preparation and Staining

To accumulate cells in metaphase 40 ng/ml of nocodazole (Sigma) was added to the exponentially growing cells for 14–16 h [Zieve et al., 1980]. To monitor the cell passage through mitosis harvested cells were washed twice with fresh medium and incubated for 0–4 h. All samples were collected during fixed time intervals. Metaphase chromosome suspensions were prepared in chromosome isolation buffer (15 mM Tris-HCl, 2 mM EDTA, 0.5 mM EGTA, 80 mM KCl, 20 mM NaCl, 0.2 mM spermine, 0.5 mM spermidine, 14 mM β-mercaptoethanol, pH 8.0). Chromosomes stained with propidium iodide (PI) in the presence of 0.25 mg/ml RNAse (Sigma) were analyzed.

Mechanical Treatment

The disperse chromosomes from mitotic cells were obtained by forcing the cell suspension through $1\frac{5}{8}''$ 25G shearing needle. The procedure was repeated until the chromosomes were free in suspension but usually not more than five times. To estimate the range of chromosome aggregates' disruption we varied the number of passages up to 40 and applied the flow cytometry analysis of each sample. Chromosomes were examined using a Zeiss Axioplan epifluorescense microscope.

Flow Cytometry

A modified ATC-3000 flow cytofluorimeter (ODAM-Brucker, France) was used. The data acquisition and accumulation were accomplished using special designed software (Dr. Klopov, Institute of Nuclear Physics RAS). The amplified signals, both the forward light scatter (488 nm) and fluorescence signals (>550 nm) were collected using additional external 12 bits ADC (L-1250S, 500 kHz, 16 channels, L-Card, Moscow), equipped with a signal processor (ADSP-2105). The analysis of chromosome sets (karyotypes) was carried out with a special device that provides the karyotypes of individual mitotic cells [Zenin et al., 1999; Zenin et al., 2001]. Numbers of expected chromosome types in each chromosome peak were calculated by relative frequency of total events of each chromosome peak in linear flow karyotypes. The peak position indicates the DNA content of the chromosome.

Computer Methods of Chromosome Clumps Prediction

The flow karyotype spectrum represents the amount of fluorescence impulses of particles (i.e., chromosomes, debris, or chromosome aggregates–clumps) in each channel [Gray et al., 1987]. Several steps were taken in order to build up a theoretical curve from the experimental one. Each experimental spectrum was split into approximated curves representing the following parameters: the number of chromosomes (the area) in each peak, the DNA content (mean) of each peak and coefficient of variation—uniformity of staining and instrument characteristic. We received a series of Gaussian distributions, one for each peak [Dean, 1985] and the exponential function to represent non-specific debris, as well as a power function to represent chromosome fragments, adding a broad Gaussian as a first approximation of chromosome clumps. Twenty-three Gaussian distribution were used for the normal karyotype, GM-130, FLECH, 25- for HEP2. The curves were built by the methods of the least squares. These data were used to generate the shape of chromosome clumps using self-made software (Dr. Klopov, Institute of Nuclear Physics RAS). The algorithm was used as following: the 1st chromosome was associated with the 2nd and we obtained a peak in the position of their summary DNA content; then the 1st with the 3rd, 4th, and so on; then the 2nd with the 3rd and so on (thus each chromosome with every other). We checked three models of chromosome clumping. In the first model, it was assumed that the probability of chromosome pair formation depended only from the area of two peaks (random clumping). The second and third models supposed that the pair formation depended on chromosome size: the probability is higher for large chromosomes (more DNA); and inverse—the probability of pairing is higher for small chromosomes (the small chromosomes in the clump are the more difficult to disrupt mechanically). At the third step, we replaced the broad Gaussian distribution used as a first approximation to obtain curve and performed a new fit using the area of this curve as a parameter. An iteration process was applied: the refined data on chromosome peaks were used to obtained refined envelope curve of doublets. No significant difference between the first curve and the refined one was found, the iteration process assumed to be unnecessary.

RESULTS

Minor Satellite and CENP-B Between the Chromosomes in Mouse Cell Line L929

The thread has been observed in various cells on metaphase plates [Takayama, 1975; Allison and Nestor, 1999]. On the chromosome spreads, the MiSat fluorescent signal is observed in the intercentromeric area connecting different chromosomes (Fig. 1Ia).

CENP-B is a commonly used centromere and prekinetochore marker, although it is absent in the neocentromere lacking satDNA [Depinet et al., 1997], which indicates that CENP-B is predominantly a satDNA-binding protein. The

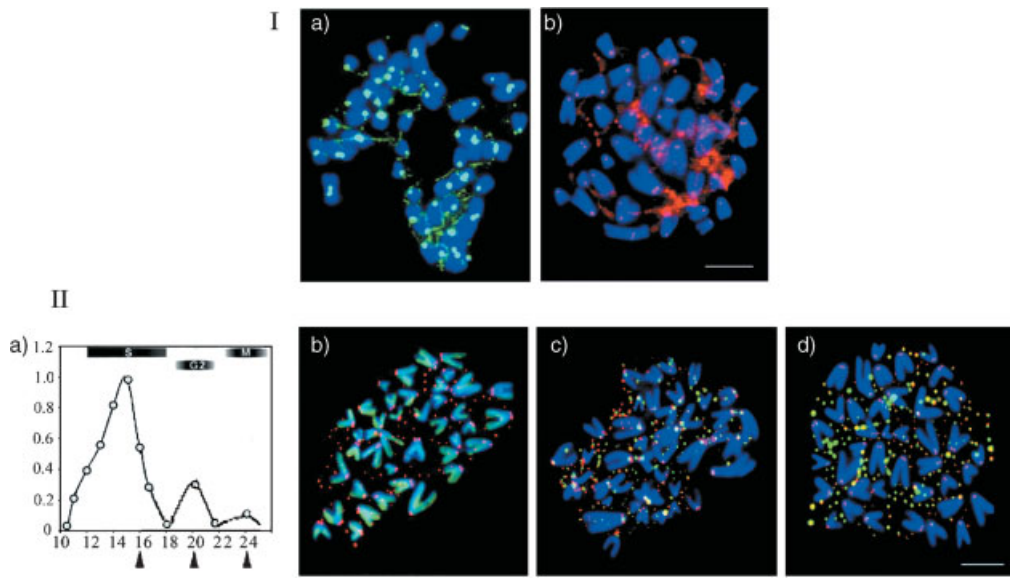

Fig. 1. **I**: Metaphase plates of mouse L929 cells hybridized with MiSat (**a**, green) and immunostained with CENP-B AB (**b**, red). DAPI pseudocolored blue. Bar is 5 μm for both images. **II**: BrdU incorporation at S and G_2/mitosis phases of mouse L929 cells. **a**: Data of FACS analysis of L929 cells synchronized in S- and G_2/M-phase. X-axis: The time of the cells incubation after serum deprivation in fresh medium (h); Y-axis, the number of events. The arrows at the bottom indicate the BrdU pulses (16, 20, and 24 h) and the letters correspond to the following images. **b–d**: Metaphase plates are immunostained with CENP-B antibody (red) and anti-BrdU antibody (green), chromosomes counterstained with DAPI (pseudocolored, blue). b: Metaphase plate from the culture BrdU pulsed at 16 h; (c) metaphase plate from the culture, BrdU pulsed at 20 h; (d) metaphase plate from the culture BrdU pulsed at 24 h. Bar is 5 μm for all images.

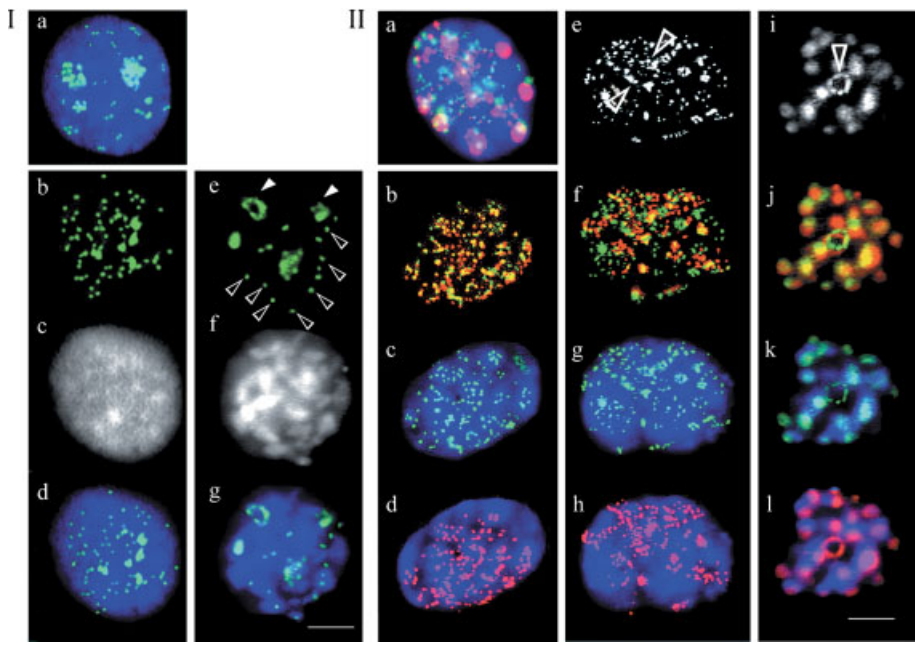

Fig. 2. **I**: Nuclear localization of Tel in the G_0/G_1 phase (**a**), G_2 phase (**b**, **c**, **d**) and at prometaphase (**e**, **f**, **g**) in the L929 cells by FISH. a: Combined images of Tel probe (green) and DAPI (blue); (b) only Tel localization (green), (c) DAPI staining in gray scale, (d) combined images of Tel probe (green) and DAPI (blue); (e) only Tel localization (green) at prometaphase, Tel fused signals are indicated by white arrows, individual signals are arranged in a circle outlined by transparent arrowheads; (f) DAPI staining in gray scale; (g) combined images of Tel probe (green) and DAPI (blue). Nuclei were counterstained with DAPI. Bar 5 is μm for all images. **II**: Double FISH with MiSat and MaSat in the L929 cells at G_0/G_1 (**a**) phase, at G_2 (**b**, **c**, **d**) phase, at prometaphase 1 (**e**, **f**, **g**, **h**) and prometaphase 2 (**i**, **j**, **k**, **l**). a: MaSat (red), MiSat (green); (c, g, k) MiSat (green) and DAPI (blue); (d, h, l) MaSat (red) and DAPI (blue); (b, f, j) MaSat (red) and MiSat (green); (e, i) only MiSat signal in gray scale is shown, on both images the arrowheads indicate the place of main thread formation. Nuclei were counterstained with DAPI (pseudocolored blue). Bar is 5 μm for all images.

thread could contain CENP-B as the thread itself bears MiSat with the CENP-B-box. The image of CENP-B staining on metaphase plate shown in Figure 1Ib. All the centromeres are labeled but distinct CENP-B signals are arranged in the same "bead-on-a-string" pattern as it was with MiSat FISH (Fig. 1Ia).

The Time of Thread Formation

The DNA of the prekinetochore domain replicates during the canonical S phase with timing similar to that of the total alpha-satellite DNA fraction [Shelby et al., 2000]. BrdU pulse-labeling used to determine the time of the thread formation. AB against CENP-B could be used to trace the thread formation according to the data in Figure 1Ib. Synchronized cells were pulsed with BrdU at hourly intervals after release into S-phase. Cells synchronized in the G_0/G_1 by serum deprivation. After release, cells proceeded through S phase, G_2/M, and into the subsequent cell cycle as assayed by flow cytometry. In 14 h after serum addition we observed enrichment in S phase, in 20 h enrichment was in G_2 (Fig. 1Ia). The corresponding metaphase plates obtained in 16, 20, and 24 h after release (Fig. 1II, arrowheads) are shown in Figure 1IIb–d. The BrdU label first belongs to the chromosomes arms (Fig. 1IIb) then to the CEN regions (Fig. 1IIc) and mostly to the foci consistent with the existence of a thread with some CENs labeled at the end (Fig. 1IId). Thus, the interchromosome connection is the last replicating DNA.

The Distribution of Telomere, Minor and Major Satellite in the G_2-Phase and at Prometaphase of Mouse L929 Cell Line

The most characteristic images of G_0/G_1 reveal the Tel hybridization signal to be clustered in large areas (Fig. 2Ia). The number of clusters per nucleus does not exceed 4 [Dolnik et al., 2003]. Distinctly paired signal spots are found in abundance on the rim of DAPI-bright chromocenters. The chromocenters, together with the Tel signal, get dispersed as the cells enter the S-phase [Kuznetsova et al., 2006b].

Tel signals have combined from a line of dots into one spot from G_2 to prometaphase (Fig. 2Ib–d). The prometaphase (Fig. 2Ie–g) is characterized by metaphase plate formation, from part of Tel together with CENs (Fig. 2Ie, transparent arrowheads underline the circle) and part of the long Tel arms form clusters. Tel clusters are dotted if in focus, two per each half of the nucleus (Fig. 2Ie, white arrowheads). They are clearly located between chromosome rosettes, indicating the association of Tel in different chromosomes into one cluster. Thus, with the Tel probe it is possible to determine the CEN arrangement in a circle, but not the thread in between.

In the G_0/G_1 phase, the MaSat hybridization signals correspond to the chromocenters to the maximum extent among the other satDNA (Fig. 2IIa). MiSat is revealed as small dots located at the chromocenter periphery (Fig. 2IIa). The overlapping of MiSat and MaSat on the rim of the chromocenters was rarely observed. MiSat arranged as "beads on a string" were observed as a network of strings connecting MaSat globules (Fig. 2IIa). The MaSat labeled chromatin occupies a large area in the interphase nuclei without full colocalization with globules of condensed heterochromatin. The pattern of fluorescent signals may vary from large to numerous small regions, occasionally interconnected with fluorescent threads (Fig. 2IIa).

MiSat and MaSat declusterization was observed during the entire S-phase [Kuznetsova et al., 2005] and in the G_2-phase both signals are visible as a number of dots abutting to each other without significant overlapping (Fig. 2IIb–d). Both signals get assembled into a more compact braid when the chromosome condensation begins (Fig. 2IIe–h). At this stage, the position of the CEN circle could be predicted (Fig. 2IIe, arrowheads). The CEN circle is clearly visible at the next stage of metaphase plate formation (Fig. 2IIi, arrowhead). We concluded that both MiSat and MaSat are involved in the thread formation though the signals do not correspond perfectly to each other.

The Localization of Telomere, Minor and Major Satellite, MS3 and MS4 on Prematurely Condensed Chromosomes

Zygote treatment with okadaic acid (a specific inhibitor of phosphoprotein phosphatases 1 and 2A) induces nuclear envelope fragmentation and premature condensation of interphase chromosomes in pronuclei as well as in second-

ary polar body nuclei [Dyban et al., 1993]. The maximal number of chromosomes in one PCC rosette does not exceed 20 as the zygotes were obtained prior to the male and female pronuclei fusion. The degree of chromosome condensation on different PCC preparations varies in the G2 phase. Chromosome condensation depends on the chromatins state at the moment of okadaic acid treatment. The chromosomes become attached to each other by the DAPI-stained DNA thread located around the "nucleolus precursor body" (Figs. 3; 4b, arrow; 6IIa, arrow; Martin et al., 2006).

The Tel repeat is not involved in the thread formation (Fig. 3a) while MaSat and MiSat participate nearly equally (Fig. 3b). All four satDNA fragments are hybridized simultaneously (Fig. 4). The PCC in Figure 4 is more condensed but less tightly bound than in Figure 3. Out of 20 chromosomes, none was lost during the metaphase plate isolation, although their integrity was slightly altered. It has been shown that the centromeric region consists of a small block of MiSat and MS3 followed by the periCEN block of MaSat with MS4 [Kuznetsova et al., 2006a]. The similarities between MaSat and MS4 (Fig. 4d1,d4) and between MiSat and MS3 (Fig. 4d2,d3) were observed and hybridization patterns are in accordance with the satDNA positions. It looks like an inner thread connects centromeres and itself is composed mostly of MiSat and MS3. On the other hand, both AT-rich satDNA (MaSat and MiSat) are more often involved in the peripheral thread formation (Fig. 4d3,d4). MS4 is involved in the thread formation to the least extent among all of satDNA fragments (Fig. 4d1).

In all cases the thread revealed by FISH is not contiguous but consists of a number of beads which are similar in size to those observed in the CEN region by fiberFISH (0.56 ± 0.08 μm for MiSat and MS3, 1.23 ± 0.13 μm for MaSat and MS4; Kuznetsova et al., 2006a).

We used PRINS on PCC in an attempt to make the order of satDNA fragments visible in the thread. An example of the results is shown in Figure 5. There is no distinct "nucleolus precursor body" on these preparations, but some group of chromosomes connected by CEN region (Fig. 5). The CEN region determined according to its position on the PCC and bright stain with DAPI. It was not fully condensed. The main part of the PRINS MiSat and MS3 signals belong to the primary constriction regions of chromosomes (Fig. 5). The PRINS signal for both fragments on PCC looks like a number of tiny dots in a dense cloud around CEN. All the chromosomes are outlined and the most heavily labeled CENs are surrounded by white transparent circles in order to attract attention to the weaker signals which belong to the thread (Fig. 5a). The heavy labeling of the CEN regions is distinct in Figure 5b,c. On all three images the threads are clearly visible as arrays of MiSat and MS3 dots. The threads are not continuous. The regular shift is obvious between MiSat and MS3 dots.

RNA Helicase p68 and CENP-B on the Prematurely Condensed Chromosomes

The thread does not consist of only DNA but also of protein [Hoskins, 1968; Saifitdinova et al., 2001]. Double immunostaining with the CENP-B and RNA helicase p68 ABs is done on compact (Fig. 6I) and more decondensed PCC (Fig. 6II). Both images show the dotted CENP-B pattern with some CENP-B involved in thread formation in the same way as on the conventional metaphase plates (Fig. 1IIb). On compact PCC it is visible that there is not only the thread between CENs but another ones connecting subtelomeric regions (Fig. 6I). CENP-B localizes to the thread in a dotted pattern in the same way as satDNA revealed with DNA-based techniques (Figs. 3, 4, 5). The main RNA helicase p68 signal belongs to the primary constriction regions of chromosomes, the interchromosome connection is followed by RNA helicase p68 and some of the RNA helicase p68 signals belong, in small amounts, to the chromosome arms (Fig. 6).

The Distribution of RNA Helicase p68 on Mitotic Chromosomes

In mitotic cells in the cell monolayer, RNA helicase p68 is found in CENs while the signal between chromosomes is even stronger (Fig. 7I). In the most preserved of chromosome spreads, RNA helicase p68 is located around the CEN region and in the thread between chromosomes (Fig. 7I,II, arrows). RNA helicase p68 staining makes not only the circle visible but also additional threads protruding from the main circle (Fig. 7IIb). Thus, RNA helicase p68 provides the network that supports the metaphase plate.

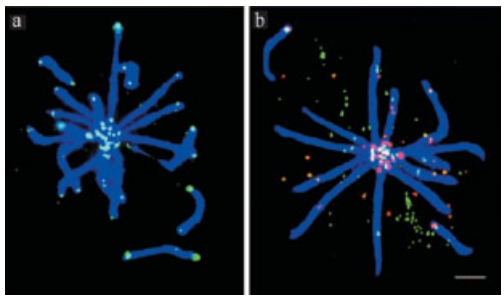

Fig. 3. FISH with the Tel (**a**), MaSat and MiSat (**b**) probes on PCC. PCC were counterstained with DAPI (pseudocolored blue). a: Tel probe (green); (b) MaSat (red) and MiSat (green). Bar is 10 μm.

Chromosome Association After Mechanical Treatment and in Mitosis Progression

The chromosome suspension is always mechanically treated, either by shearing needle or vortexing before FACS. During the standard preparation of chromosomes for FACS, the part of the flow karyotype spectrum that is usually unexamined (that on the right-hand side) always contains chromosome particles remaining after mechanical treatment. These particles may consist of debris as well as associated chromosomes.

In this part of the work we tried to find out if it was possible to separate chromosomes from

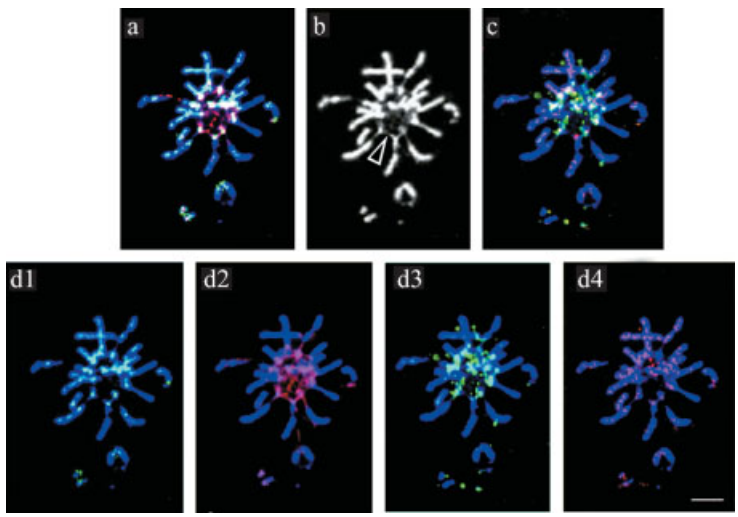

Fig. 4. FISH with all four mouse satDNA fragments on PCC. **a**: MS4 (green) and MS3 (red); (**b**) only DAPI in gray scale, arrow points at chromosome connection; (**c**) MiSat (green) and MaSat (red). **d1**: Only MS4 (pseudocolored green); (**d2**) MS3 (pseudocolored red); (**d3**) MiSat (pseudocolored green); (**d4**) MaSat (pseudocolored red). PCC were counterstained with DAPI (pseudocolored blue). Bar is 10 μm for all images.

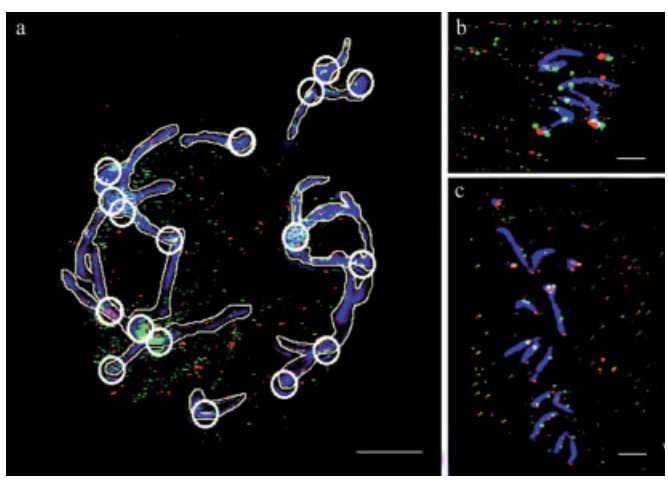

Fig. 5. PRINS on PCC with primers to CEN satDNA fragments: MiSat (red) and MS3 (green). **a**: The whole metaphase plate; (**b**, **c**) fragments from two other metaphase plates. Chromosomes bodies are outlined and CENs are in circles on ''a.'' DAPI pseudocolored blue. Bar is 10 μm for ''a'' and 5 μm for ''b, c.''

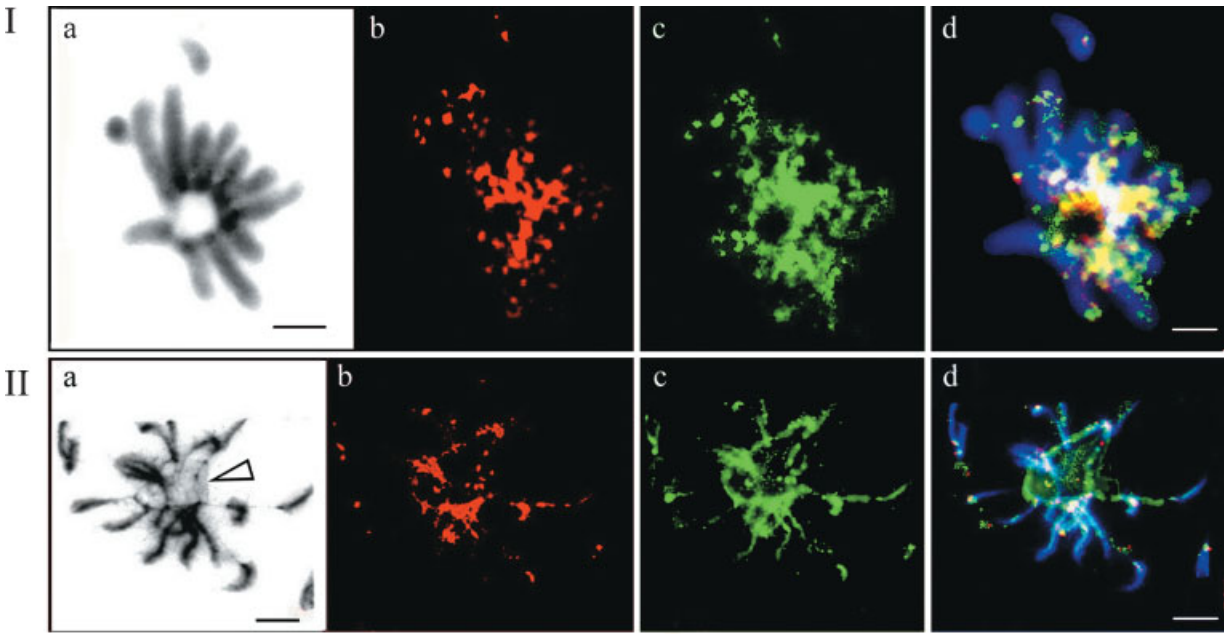

Fig. 6. Compact (**I**) and dispersed (**II**) PCC double immunostained with AB against CENP-B and AB against RNA helicase p68. **a**: DAPI in gray scale; (**b**) CENP-B (red); (**c**) RNA helicase p68 (green); (**d**) merged images, CENP-B (red), RNA helicase p68 (green). DAPI pseudocolored blue. At II, (a) arrow points at chromosome connection. Bar is 10 μm.

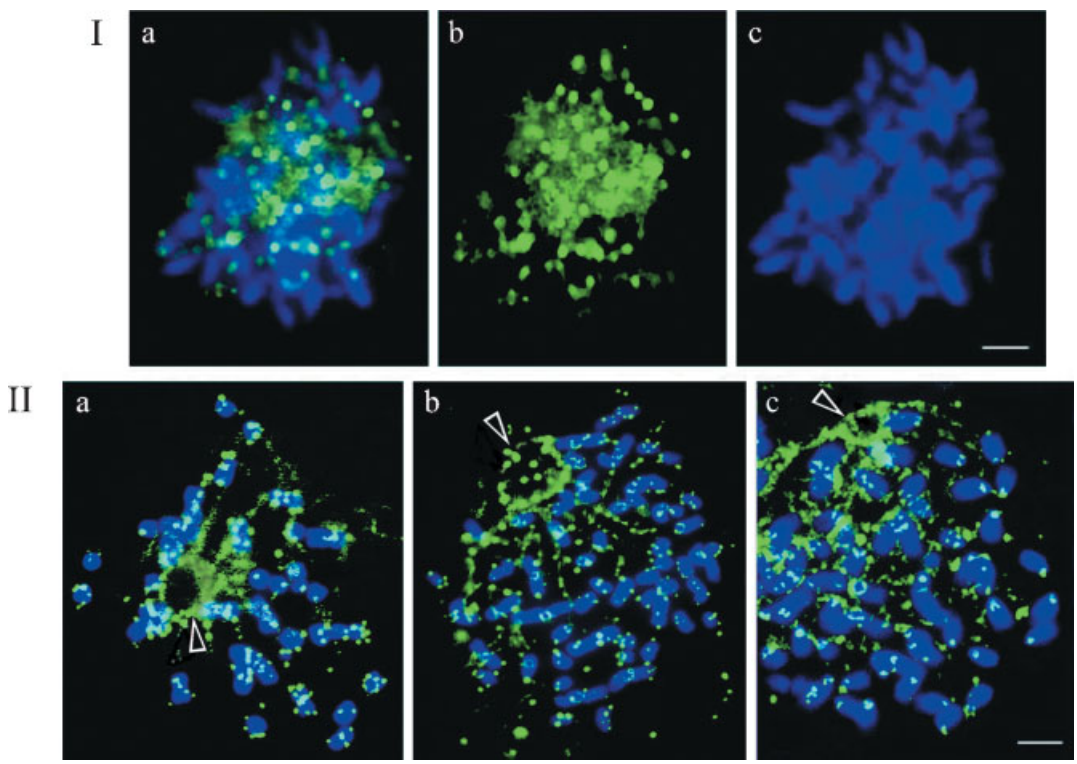

Fig. 7. RNA helicase p68 localization on metaphase chromosome spreads from the cells. **I**: Mitotic cell from the cell culture monolayer. **a**: Combined images of RNA helicase p68 (green) and DAPI (pseudocolored blue); (**b**) only RNA helicase p68 (green); (**c**) DAPI (pseudocolored blue). Chromosomes were counterstained with DAPI. Bar is 5 μm for all images. **II**: Mitotic plates obtained by spreading. Combined images of RNA helicase p68 (green) and DAPI (pseudocolored blue). The transparent arrowheads indicate the place of thread formation. Chromosomes were counterstained with DAPI. Bar is 5 μm for all images.

both the debris and the chromosomes aggregates (clumps) by FACS and to define the sufficient degree of mechanical treatment in order to analyze the chromosome suspensions subjected to FACS. The analysis of chromosome aggregates was carried out not only in mitosis but in the mitotic progression under standard conditions of preparing a chromosome suspension for FACS. Human cell lines with a well-studied flow karyotype were used (Hep-2, GM-130, FLECH).

The particles (i.e., chromosomes, debris, or chromosome aggregates—clumps) are estimated after a number of passages through the shearing needle. The amount of chromosome aggregates decreases up to 6–10 passages but the preparations are never completely free of aggregates (Fig. 8A). After 40 passages the amount of debris increased significantly (Fig. 8A). So the mechanical treatment was fixed at 10 shearing needle passages for these experiments. It is possible to increase the mechanical treatment to some level, after which the destruction of the chromosomes occurs and the clumps still exist. So the durability of connection is comparable with durability of chromosome itself. For the mitotic arrest the cells was treated with nocodazole, which prevents tubulin polymerization. Chromosomes are not held together by spindle in such a case, so spindle components do not responsible for the aggregates formation.

The transition from metaphase to anaphase was checked at different times after cytostatic removal with fixed mechanical treatment (Fig. 8B). Chromosomes gradually split into chromatids as mitosis proceeds but the ratio between chromosomes and aggregates remains constant (Fig. 8B; Table I). Thus, by FACS we demonstrated that the amount of chromosome association decreases from mitosis to interphase (Table I).

Analysis of Chromosome Associations in the Different Cell Lines by FACS

Examples of the typical flow karyotypes for different human cell lines are shown in Figure 9A. In all cases the conventional spectrum comparable with the data published [Dean, 1985; Lee et al., 2000] has been obtained and, in each case, the spectrum contains chromosome aggregates (clumps) as expected on the right-hand part (Fig. 9A, brackets).

The possible variations of chromosome associations were mathematically analyzed (see Materials and Methods). The parameters of interest were the number of chromosomes in each peak and its DNA content. Theoretical curves of chromosome distribution in clumps have been built on the assumptions that either of two chromosomes could be associated with equal probability. The algorithm was as follows: the first chromosome aggregates are taken with the second and a peak in the position of their summary DNA content is obtained. Then the first with the third followed by the first with the fourth and so on. The process is repeated so that each chromosome is matched with each other. All the peaks from chromosome doublets are

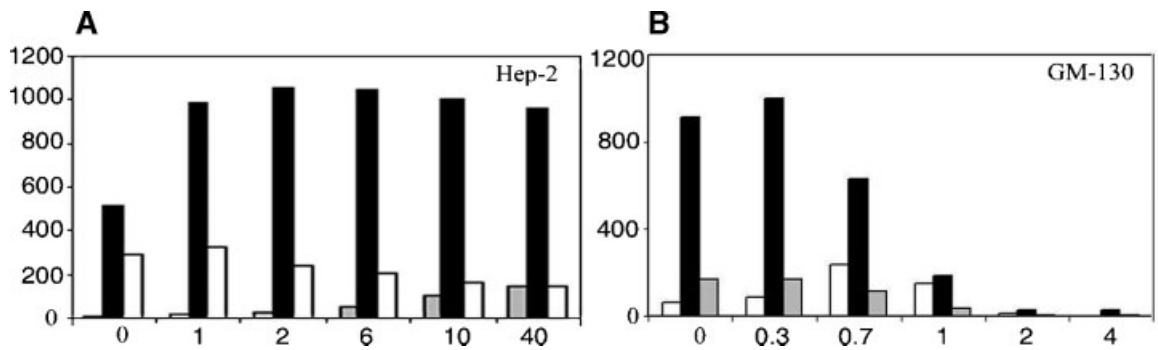

Fig. 8. The relative amount of discrete particles in chromosome suspension during mechanical treatment (**A**) and mitosis progression (**B**) in the human Hep-2 and GM-130 cell lines by FACS. A: Y-axis, the amount of DNA particles in μm^3 (chromosomes, aggregates of chromosomes, chromosome fragments or debris); X-axis, the number of passages through a shearing needle. The white column, chromosomes aggregates; the black column, chromosomes; the gray column, debris. B: Y-axis, the amount of DNA content particles in μm^3; X-axis, the time of cell incubation after nocodazole removal in fresh medium for 0, 0.3, 0.7, 1, 2, 4 h. The number of passages through a shearing needle was fixed at 10 according to results in **1A**. The black column, chromosomes; the white column, chromatides; the gray column, aggregates. The aggregates/chromosomes are shown in Table I.

TABLE I. The Amount of the Aggregates and Aggregate/Chromosome Ratio in Mitosis Progression of GM-130 Cell Line

The time of incubation (hours)	0	0.3	0.7	1	2	4
The amount of the aggregates (μm^3)	166	165	118	34	3	5
Aggregates/chromosomes ratio	0.181	0.165	0.186	0.185	0.132	0.169

The time of the cells incubation after nocodazole removal in hours (see Fig. 8B). The amount of the aggregates was counted in μm^3. The ratio of aggregates to chromosomes is in relative units.

summarized and we obtain a theoretical curve. In the model used (random clumping), it was assumed that the probability of chromosome pair formation depended only on the area of two peaks. The theoretical curve forecast was then compared with the experimental one for different cell types.

Clumps containing part of the flow karyotypes (Fig. 9A, brackets) together with the theoretical curves are shown in Figure 9B. The obvious clumps are situated on the right of the flow karyotype spectrum, with the DNA content being higher than that of the largest chromosomes. The best coincidence of the experimental and the theoretical curves is observed when the latter was based on the supposition of random (equiprobable) chromosome association (Fig. 9B).

Examples of karyotypes from 5 GM-130 individual mitotic cells are shown in Figure 9, Cb. In such a case each chromosome or clump is represented by a column with the length dependent on its DNA content. Nor a single one of the one-cell karyotypes contains the amount of chromosomes characteristic of this cell line. The chromosome mode of the line GM-130 subjected to "one-cell flow karyotype" has been determined (46 chromosomes). But one-cell karyotypes never show the same number (<46 chromosome) because of the presence of chromosomes aggregates. If a number of GM-130 one-cell karyotypes (Fig. 9Ca) are summarized, the resulting curve will correspond to the ordinary flow karyotype of the same cell line (Fig. 9A, GM-130). One-cell karyotypes also contain aggregates as is shown for flow karyotype (Fig. 9Cb, GM-130) and interchromosome connections exist in every metaphase plate.

The flow karyotype of the mouse L929cell line, which was used in the previous part of the work is shown in Figure 9Da. The well-distinguished peak consists of separate chromosomes combined according to its length and DNA content (Fig. 9Da; 10f). At the right part of the L929 spectrum (Fig. 9Da) the same tendency as with human cells is visible, that is, the karyotype contains a number of clumps (Fig. 9Db). The cytological analysis of the L929 chromosomes for FACS (Fig. 10) in the shearing needle experiments demonstrated the same tendency as in the human cell lines (Fig. 8A). The interchromosome connections are easy to observe on PI-stained chromosome plates during its preparation for FACS by epifluorescense microscopy (Fig. 10c,d, arrows).

The flow karyotype of 6×10^8 cells for each cell type was studied. The interaction between chromosomes in mitosis is random but regular both in the cells of human culture and in mice cells whose chromosomes are difficult to resolve by FACS.

DISCUSSION

Chromosome Positions at Metaphase, Thread Establishment and Post-Mitotic Fate

The debates about the existence of the thread between chromosomes could not be separated from the long-standing question about chromosome order in the mitotic ring and interphase nuclei. In 1885, Rabl suggested that the radial chromosomal positions on the mitotic ring during mitosis were a reflection of the relative chromosomal positions at the preceding interphase [Rabl, 1885]. The prophase movements of chromosomes support this view, as there are no wide shifts in the positions of the prophase chromosomes relative to each other as they move to the metaphase plate [Bajer and Molè-Bajer, 1981; Chaly and Brown, 1988; Hiraoka et al., 1990]. The time of chromosome reshuffling corresponds or is very close to the moment of the thread replication, that is, its final formation (Fig. 1II). Our data can explain the small peak of H^3-thymidine uptake regularly observed in the G_2-phase [Blyumkin and Ulyanova, 1976; Shelby et al., 2000]. The thread is the last replicating DNA just before mitosis and it fixes the chromosome order in the mitotic ring. It is proposed that chromosome-specific timing of sister chromatid separation transmits the chromosomal position from one cell genera-

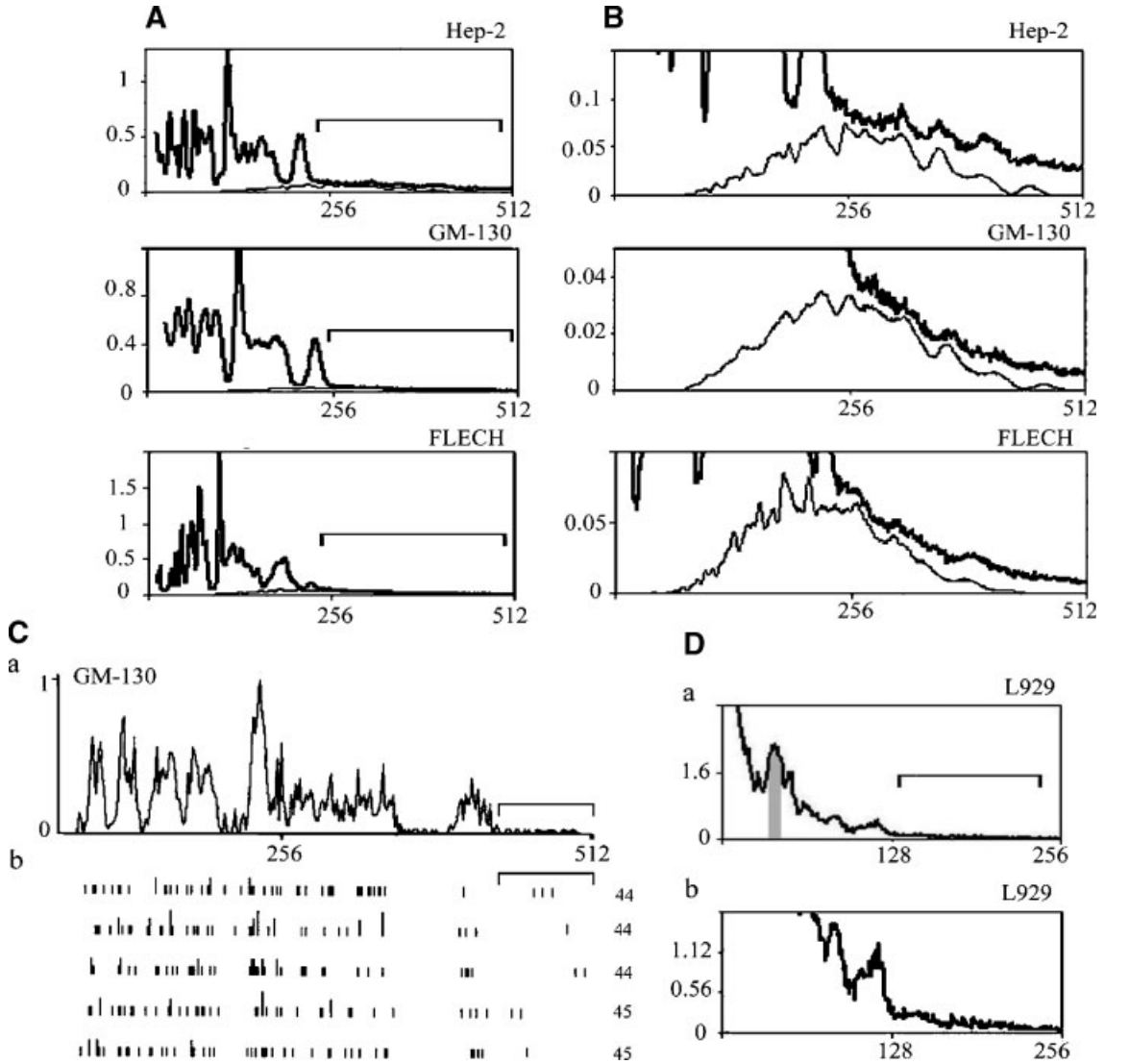

Fig. 9. The experimental histograms of flow karyotypes of different cell lines (see Materials and Methods). The name of each cell line is indicated on the left of each square at the top. **A**: The flow karyotypes of three cell lines: Hep-2, GM-130, FLECH. X-axis: The DNA fluorescence intensity (DNA relative content) in arbitrary units (a.u.); Y-axis, the number of events. The ''independent event'' is the expectancy to meet DNA content particles (chromosomes, aggregates of chromosomes, debris) in each channel. The brackets indicate area of chromosomes aggregates only. **B**: The part of the same histograms (A) with chromosomes aggregate regions are shown at high magnification. The experimental curves of the histograms are clipped to magnify aggregate regions (the bold line) combined with theoretical curves (the regular line) of aggregate built up on the assumption that each chromosome is free to associate with every other. X-axis: The DNA relative content (a.u.); Y-axis, the number of events. **C**: Comparison between the standard flow karyotype of GM-130 cell line (**a**) and the flow karyotype of five individual cells (**b**). a: Standard flow karyotype of GM-130 cell line. X-axis: The DNA relative content (a.u.); Y-axis, the number of events. **b**: Compact representation of the flow karyotype of five individual cells. Each row represents the individual karyotype of a cell. Chromosomes or aggregates in the channel are shown as a vertical black line with a certain length depending on DNA content, which determines the chromosome position of the line on X-axis in (a). The vertical black line is the length representing the mean peak of each chromosome. The figures on the right show the number of chromosomes in each given set. The brackets indicate the aggregate region (clumps). **D**: The experimental flow karyotype of mouse L929 cells (**a**), the part of the same histograms with aggregates region is shown at high magnification (**b**). The bracket indicates the aggregates region. X-axis: The DNA relative content (a.u.); Y-axis, the number of events. The area of separate chromosomes is indicated as a gray column shown in (a). The chromosomes from this area are demonstrated in Figure 10f.

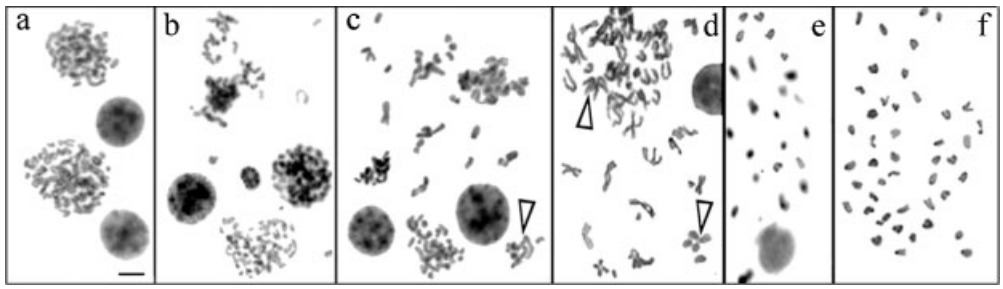

Fig. 10. The analysis of L929 chromosome prepared for FACS in the shearing needle experiments. Chromosomes stained with PI, inverted image. **a**: 0 passage through a shearing needle in Figure 8A; (**b**) 1 passage through shearing needle, that is, cells went trough a syringe needle once; (**c**) 6 passages through shearing needle; (**d**) 10 passages through shearing needle; (**e**) 40 passages through shearing needle; (**f**) separate L929 chromosomes after FACS from the fraction indicated in Figure 9Da. Arrows on ''c'' and ''d'' indicate chromosome clumps. Bar is 5 μm for all images.

tion to the next, based on tracing of labeled chromosomes and centromeres during chromosome segregation and experimental perturbations of chromosomal order [Gerlich et al., 2003].

Although metaphase [Maniotis et al., 1997a] and interphase chromosomes are connected to each other [Bolzer et al., 2005], if not by nucleotide strands then by DNA–protein complexes [Maniotis et al., 1997b], there is no evidence that such connections are permanent. If the fixed order of the relative positions of chromosomes on the mitotic ring were maintained from the initial fusing of parental haploid genomes into the next meiotic division, the random Mendelian segregation of chromosomes could not occur. We can thus conclude that the thread is destroyed at the end of karyokinesis.

We examined mouse mitotic cells by FISH and PRINS with different combinations of all four satDNA probes. We noticed that chromatid cohesion is sustained for a longer time in the periCEN region (MaSat + MS4) when compared with CEN (MiSat + MS3) according to the data published [Guenatri et al., 2004]. However, we failed to determine any thread in between unfolding chromosomes (data not shown). On the other hand, the midbody in between the daughter cell contains DNA-binding proteins, that is, DNA-remodeling factors [Sigala et al., 2005]. The supposition to check is whether part of the thread goes to the midbody in between the daughter cell during karyokinesis.

Our results demonstrated that all possible chromosomal arrangements occur on the mitotic ring though the amount of the chromosome aggregates decreases in the mitotic progression (Fig. 8B; Table I) in agreement with the previous findings [Allison and Nestor, 1999]. It has been assumed that clumps are the result of insufficient mechanical treatment of the metaphase plate, but it is not so (Fig. 8 and 9). The mechanical treatment of metaphase plates and the observation of the chromosome state during mitosis lead to the conclusion that aggregates exist as long as chromosomes exist. The durability of the connection between chromosomes is comparable with that of chromosomes themselves. Still the overwhelming majority of the flow karyotypes show clumps, the number of which varies in different experiments. Different conditions, that is, RNase [Van den Engh et al., 1984], protease [trypsin, Trask et al., 1989] and mechanical treatment reduce the amount of clumps, but do not destroy them completely.

Chromosomes within the pronucleus are randomly positioned relative to each other [Dozortsev et al., 2000]. Nonrandom chromosomal associations on the mitotic ring are reported for some cell types [Kuwano et al., 1992; Nagele et al., 1995]. It was supposed that small chromosomes were more likely to be involved in association [Van den Engh et al., 1984; Lee et al., 2000]. In contrast to this supposition, the clump formation in our experiments does not depend on the chromosome length. The traditional flow karyotype based on prepared chromosome suspension could not shed light on whether clumps exist in each cell or only some "defective" metaphase plates contribute to the clump formation. The results of "one cell flow karyotypes" analysis show that chromosomes are associated and their association does not depend on the chromosome length (Fig. 9C). One-cell karyotype as well as the flow karyotype

was showing inevitable clumping. So FACS indicates that interchromosome connection exists in vivo.

DNA and Protein Thread Composition

Tel was never involved in the thread formation despite the previous supposition made by Poirier and Marko [2002]. CEN and periCEN satDNA both were found to be necessary components of the thread. There was a difference in the amount of these satellites. On ordinary metaphase plates of mouse L929 hybridized with MiSat and stained with anti-CENP-B, the thread between chromosomes was visible but often lost in image processing as a weak signal. Signals outside CEN was counted as nonspecific staining. The intermingling order of MiSat and MS3 is obvious along the thread (Fig. 5b,c). Previously we demonstrated that the CEN region consists of intermingling small MiSat and MS3 blocks followed by intermingling periCEN MaSat with MS4 blocks [Kuznetsova et al., 2006a]. Thus we assume that the thread is built up of DNA similar to that of CEN and, probably, derived from CEN. This supposition could get its confirmation with probes, which will cover the whole CEN region.

Conventional mitotic spread did not give resolution, which could be achieved on PCC. Lack of perfect CEN condensation makes the PRINS signal on PCC different from the FISH one on the conventional metaphase spread (Fig. 1Ia). Probably, the interval between the fragments depends on the force applied to PCC, which could not be controlled during the preparation. The thread could not be in a fully condensed state due to the treatment with okadaic acid but at least CEN satDNA fragments are arranged in the thread in intermingling order.

CENP-B presence in the thread followed the MiSat involvement in the thread formation. The CENP-B signal was very similar to that of the MiSat FISH signal (Fig. 1I). SatDNA-binding protein, CENP-B [80 kDa; Earnshaw and Rothfield, 1985] binds the 17-bp CENP-B box (xTTCGxxxxAxxCGGGx) within human α-sat DNA and mouse MiSat monomers [Muro et al., 1992; Sugimoto et al., 1998]. It has been shown to bind centromeric satDNAs only. CENP-B presence in the thread confirms that the thread is built up of the DNA similar to that of CEN.

We also found another protein within the thread: RNA helicase p68. We purified RNA helicase RNA from the mouse nuclear matrix using ion-exchange and affinity chromatography as the main MiSat binding protein in vitro [Enukashvily and Podgornaya, 2001]. At mitosis RNA helicase p68 was found in both the CEN and periCEN regions and the connections between chromosomes. In accordance with RNA helicase p68 specificity in binding to different satDNA [Podgornaya et al., 2000, 2003], it stained the thread more smoothly than CENP-B (Fig. 6). However, the large portion of the RNA helicase p68 colocalizes with CENP-B. Proteins were arranged as beads (Fig. 6I) along the thread in the same way as satDNA. CENP-B was involved in the thread formation in the same way as was seen with conventional methaphase spread though to a lesser extent than RNA helicase p68 (Fig. 6IIb). The shape of the circle revealed with RNA helicase p68 AB is very similar to that observed with the satDNA label (Fig. 2IIe,i, arrows).

Almost 10 years ago the importance of RNA polymerase II for heterochromatin maintenance was demonstrated in mammals [Haaf and Ward, 1996]. Recently, it has become obvious that heterochromatin formation depends on the RNA interference (RNAi) machinery in fission yeast (*S. pombe*). The mammalian RNAi pathway is essential for differentiation and chromatin structure maintenance [Kanellopoulou et al., 2005]. The RNAi heterochromatization machinery is ribonucleoprotein complexes which contain helicases. The *Drosophila* homolog of RNA helicase p68 (Dmp68) is required for efficient RNAi [Ishizuka et al., 2002].

The chromatin in the thread is not heterochromatic during mitosis though it is formed on the base of satDNA, which was heterochromatic at the interphase. The recovery of the heterochromatic state must be done quickly—somewhere between anaphase and the very beginning of the interphase. Therefore, the components of heterochromatinization machinery (e.g., RNA helicase) should follow the thread to speed up the heterochromatinisation; they are necessary for epigenetic marking the DNA of the thread as heterochromatic. The next experimental question to address is whether the proteinaceous component of the thread contains any other proteins from the RNAi pathway of heterochromatization.

ACKNOWLEDGMENTS

The MiSat containing plasmid was the kind gift of Dr. D. Kipling (HGU MRC, Western General Hospital, Edinburgh, UK). The MaSat containing plasmid was kindly provided by Dr. B. Hamkalo (Department of Molecular Biology and Biochemistry, University of California). The telomere probe was a generous gift from Dr. Gilson (Ecole Normale Superieure de Lyon, France). We are grateful to Ms. Sheila Lemoin (Manchester, UK) for the English corrections. The work was supported in part by the Joint Research Center "Material Science and Characterization in High Technology."

REFERENCES

Allison DC, Nestor AL. 1999. Evidence for a relatively random array of human chromosomes on the mitotic ring. J Cell Biol 145:1–14.

Bajer AS, Molè-Bajer J. 1981. Mitoses: Studies of living cells: A revision of basic concepts. In: Zimmerman AM, Forer A, editors. In mitoses/cytokineses. New York: Academic Press. p. 227–299.

Blyumkin VN, Ulyanova LI. 1976. The action of heparin on the incorporation of thymidine-H^3 in the cells of the continuous line A-1. Bull Exp Biol Med 9:1119–1121.

Bolzer A, Kreth G, Solovei I, Koehler D, Saracoglu K, Fauth C, Muller S, Eils R, Cremer C, Speicher MR, Cremer T. 2005. Three-dimensional maps of all chromosomes in human male fibroblast nuclei and prometaphase rosettes. PloS Biol 3:0826–0842.

Chaly N, Brown DL. 1988. The prometaphase configuration and chromosome order in early mitosis. J Cell Sci 91: 325–335.

Chiarelli B, Ardito G, Brogger A. 1977. The non-random distribution of human chromosomes at metaphase: II. Interchromosome connections. Nucleus 20:249–251.

Cohen P, Holmes CF, Tsukitani Y. 1990. Okadaic acid: A new probe for the study of cellular regulation. Trends Biochem Sci 15:98–102.

Dean PN. 1985. Helpful hints in flow cytometry and sorting. Cytometry 6:62–64.

Depinet TW, Zackowski JL, Earnshaw WC, Kaffe S, Sekhon GS, Stallard R, Sullivan BA, Vance GH, van Dyke DL, Willard HF, Zinn AB, Schwartz S. 1997. Characterization of neocentromeres in marker chromosomes lacking detectable alpha-satellite DNA. Hum Mol Genet 6:1195–1204.

Dolnik AV, Kuznetsova IS, Voronin AP, Podgornaya OI. 2003. Telomere-binding TRF2/MTBP localization during mouse spermatogenesis and cell cycle of the mouse cells L929. J Anti Aging Med 6:107–121.

Dozortsev D, Coleman M, Nagy P, Diamond M, Ermilov A, Weier U, Liyanage M, Reid T. 2000. Nucleoli in a pronuclei stage mouse embryo are represented by major satellite DNA of interconnecting chromosomes. Fertil Steril 73:366–371.

Dyban AP, de Sutter P, Verlinsky Y. 1993. Okadaic acid induces premature chromosome condensation reflecting the cell cycle progression in one-cell stage mouse embryos. Mol Reprod Dev 34:402–415.

Earnshaw WC, Rothfield N. 1985. Identification of a family of human centromere proteins using autoimmune sera from patients with scleroderma. Chromosoma 91:313–321.

Earnshaw WC, Ratrie H, Stetten G. 1989. Visualization of centromere proteins CENP-B and CENP-C on a stable dicentric chromosome in cytological spreads. Chromosoma 98:1–12.

Enukashvily N, Podgornaya O. 2001. The murine nuclear matrix protein specifically binds to centromeric satellite DNA. Tsitologia 43:52–60.

Enukashvily NI, Lobov IB, Kukalev AS, Podgornaya OI. 2000. A nuclear matrix protein related to intermediate filaments proteins is a member of the complex binding alphoid DNA in vitro. Cell Biol Int 24:483–492.

Enukashvily N, Donev R, Sheer D, Podgornaya O. 2005. Satellite DNA binding and cellular localisation of RNA helicase p68. J Cell Sci 118:611–622.

Gerlich D, Beaudouin J, Kalbfuss B, Daigle N, Eils R, Ellenberg J. 2003. Global chromosome positions are transmitted through mitosis in mammalian cells. Cell 112:751–764.

Gooderham K, Jeppesen P. 1983. Chinese hamster metaphase chromosomes isolated under physiological conditions. A partial characterisation of associated non-histone proteins and protein cores. Exp Cell Res 144: 1–14.

Gray JW, Dean PN, Fuscoe JC, Peters DC, Trask BJ, van den Engh GJ, van Dilla MA. 1987. High-speed chromosome sorting. Science 238:323–329.

Guenatri M, Bailly D, Maison C, Almouzni G. 2004. Mouse centric and pericentric satellite repeats form distinct functional heterochromatin. J Cell Biol 166:493–505.

Haaf T, Ward DC. 1996. Inhibition of RNA polimerase II transcription causes chromatin decondensation, loss of nucleolar structure, and dispersion of chromosomal domains. Exp Cell Res 224:163–173.

Hiraoka Y, Agard DA, Sedat JW. 1990. Temporal and spatial coordination of chromosome movement, spindle formation, and nuclear envelope breakdown during prometaphase in Drosophila melanogaster embryos. J Cell Biol 111:2815–2828.

Hoskins GC. 1968. Sensitivity of micrurgically removed chromosomal spindle fibres to enzyme disruption. Nature 217:748–750.

Ishizuka A, Siomi MC, Siomi H. 2002. Drosophila fragile X protein interacts with components of RNAi and ribosomal proteins. Genes Dev 16:2497–2508.

Kanellopoulou C, Muljo SA, Kung AL, Ganesan SH, Drapkin R, Jenuwein T, Livingston DM, Rajewsky K. 2005. Dicer-deficient mouse embryonic stem cells are defective in differentiation and centromeric silencing. Genes Dev 19:489–501.

Kipling D, Mitchell AR, Masumoto H, Wilson HE, Nicol L, Cooke HJ, 1995. CENP-B binds a novel centromeric sequence in the Asian mouse *Mus caroli*. Mol Cell Biol 15:4009–4020.

Kuwano A, Matsuura S, Kajii T. 1992. Telomere association of human chromosomes induced by aphidicolin. Mutat Res 269:107–111.

Kuznetsova IS, Prusov AN, Enukashvily NI, Podgornaya OI. 2005. New type of the mouse centromeric satellite DNA. Chromosome Res 13:9–25.

Kuznetsova I, Podgornaya O, Ferguson-Smith MA. 2006a. High-resolution organization of mouse centromeric and pericentromeric DNA. Cytogenet. Genome Res 112:248–255.

Kuznetsova IS, Voronin AP, Podgornaya OI. 2006b. Telomere and TRF2/MTBP localization in respect to satellite DNA during the cell cycle of mouse cell line L929. Rejuvenation Res 9(3):391–401.

Lee JH, Arumuganathan K, Chung YS, Kim KY, Chung WB, Bae KS, Kim DH, Chung DS, Kwon OC 2000. Flow cytometric analysis and chromosome sorting of barley (*Hordeum vulgare* L). Mol Cells 10:619–625.

Maniotis AG, Bojanowski K, Ingber DE. 1997a. Mechanical continuity and reversible chromosome disassembling within intact genomes rendered from living cells. J Cell Biochem 65:114–130.

Maniotis AG, Chen CS, Ingber DE. 1997b. Demonstration of mechanical connections between integrins, cytoskeletal filaments, and nucleoplasm that stabilize nuclear structure. Proc Natl Acad Sci USA 94:849–854.

Martin C, Beaujean N, Brochard V, Audouard C, Zink D, Debey P. 2006. Genome restructuring in mouse embryos during reprogramming and early development. Dev Biol 292:317–332.

Mitchell AR, Jeppesen P, Nicol L, Morrison H, Kipling D. 1996. Epigenetic control of mammalian centromere protein binding: Does DNA methylation have a role. J Cell Sci 109:2199–2206.

Muro Y, Masumoto H, Yoda K, Nozaki N, Ohashi O, Okazaki T. 1992. Centromere protein B assembles human centromeric alpha-satellite DNA at the 17-bp sequence, CENP-B box. J Cell Biol 116:585–596.

Nagele RG, Freeman T, McMorrow L, Lee HY. 1995. Precise spatial positioning of chromosomes during prometaphase: Evidence for chromosomal order. Science 270:1831–1835.

O'Keefe RT, Henderson SC, Spector DL. 1992. Dynamic organization of DNA replication in mammalian cell nuclei: Spatially and temporally defined replication of chromosome-specific alpha-satellite DNA sequences. J Cell Biol 116:1095–1110.

Podgornaya O, Dey R, Lobov I, Enukashvili N. 2000. Human satellite 3 (HS3) binding protein from the nuclear matrix: Isolation and binding properties. Bioch Biophys Acta 1497:204–214.

Podgornaya OI, Voronin AP, Enukashvily NI, Matveev IV, Lobov IB. 2003. Structure-specific DNA-binding proteins as the foundation for 3-dimensional chromatin organization. Int Rev Cytol 224:227–296.

Poirier MG, Marko JF. 2002. Micromechanical studies of mitotic chromosomes. J Muscle Res Cell Motil 23:409–431.

Rabl C. 1885. Uber zelltheilung. Morphol Jahrbot 10:214–330.

Radic MZ, Lundgren K, Hamkalo BA. 1987. Curvature of mouse satellite DNA and condensation of heterochromatin. Cell 50:1101–1108.

Saifitdinova A, Derjusheva S, Malykh A, Zhurov T, Andreeva TF, Gaginskaya ER. 2001. Centromeric tandem repeat from the chaffinch genome: Pisolation and molecular characteristization. Genome 44:96–103.

Shelby RD, Monier K, Sullivan KF. 2000. Chromatin assembly at kinetochores is uncoupled from DNA replication. J Cell Biol 151:1113–1118.

Sigala B, Edwards M, Puri T, Tsaneva IR. 2005. Relocalization of human chromatin remodeling cofactor TIP48 in mitosis. Exp Cell Res 310:357–369.

Sugimoto K, Shibata A, Himeno M. 1998. Nucleotide specificity at the boundary and size requirement of the target sites recognized by human centromere protein B (CENP-B) in vitro. Chromosome Res 6:133–140.

Takayama S. 1975. Interchromosomal connections in squash preparations of L cells. Exp Cell Res 91:408–412.

Trask B, van den Engh G, Mayall B, Gray JW. 1989. Chromosome heteromorphism quantified by high-resolution bivariate flow karyotyping. Am J Hum Genet 45: 739–752.

Van den Engh G, Trask B, Cram S, Bartholdi M. 1984. Preparation of chromosome suspensions for flow cytometry. Cytometry 5:108–117.

Zenin VV, Aksenov ND, Shatrova AN, Klopov NV, Kram LS, Poletaev AI. 1999. A device for sample pretreatment during flow cytometry. Biofizika (Moskow) 44:303–312.

Zenin VV, Klopov NV, Drbchenko ND, Aksenov ND, Shatrova AN, Poletaev AI. 2001. Mitotic cell analysis by means of univariate flow cytometry. Biologicheskie Membrani (Moskow) 18:207–215.

Zieve GM, Turnbull D, Mullins JM, Mclntosh JRZ. 1980. Production of large numbers of mitotic mammalian cells by use of the reversible microtubule inhibitor nocadazole. Exp Cell Res 126: 397–405.